

# Design and analysis of corner scatter inclusion in photonic crystal-based ring resonator

ANUSOOYA VADUKANATHAN<sup>1,\*</sup>, GOBALAKRISHNAN SUYAMBRAKASAM<sup>2,\*</sup>,  
PONMALAR SIVARAJ<sup>3</sup>, MANIKANDAN MOOLA SEETHARAMAIER KASIVISWANATHAN<sup>4</sup>

<sup>1</sup>Department of Electronics and Communication Engineering, SRM Institute of Science and Technology, Kattankulathur, Chengalpattu District, Chennai, Tamil Nadu 603203, India

<sup>2</sup>Department of Humanities and Science (Physics), Rajalakshmi Engineering College, Rajalakshmi Nagar, Thandalam, Kanchipuram District, Tamil Nadu 602105, India

<sup>3</sup>Department of Computer Science and Engineering, Velammal College of Engineering and Technology, Viraganoor, Madurai, Tamilnadu 625009, India

<sup>4</sup>Department of Electronics and Communication Engineering, Thiagarajar College of Engineering, Madurai, Tamilnadu 625015, India

\*Corresponding authors: prof.v.anusooya@gmail.com (AV), gobalphd@gmail.com (GS)

One of the significant challenges in integrated optical systems is achieving miniaturization. Traditional components can limit the effective utilization of chip area. Devices with distinctive thickness and length characteristics, including the Mach Zehnder interferometer (MZI), the directional coupler, and waveguides, contribute to this issue, limiting the efficient use of chip area. Photonic crystals offer a solution to this problem. The proposed design results in two optical bandgap ranges, from 0.456586 to 0.675819  $\mu\text{m}^{-1}$  and from 1.12855 to 1.16338  $\mu\text{m}^{-1}$ , both in TE mode with gap widths of 0.219233 and 0.34826  $\mu\text{m}^{-1}$ , respectively. The corresponding wavelength ranges are from 1479 to 2190 nm and 859 to 886 nm. The analysis of field propagation in the photonic crystal ring resonator (PCRR) is carried out using the finite-difference time domain (FDTD) method, while the bandgap analysis is performed by the plane wave expansion (PWE) method. This work primarily focuses on the incorporation of corner scatters in the PCRR. Corner scatters play a crucial role in guiding the field smoothly inside the ring, thus preventing the localization of light within the structure. After the simulation, various attributes were compared for both structures. At a resonant wavelength of 1550 nm, the input intensity is measured as 0.0591 a.u., and the output intensities for with and without corner scatter are 0.0458 and 0.0539 a.u., respectively.

Keywords: photonic crystal ring resonator, corner scatter, FDTD, photonic bandgap, plane wave expansion.

## 1. Introduction

Ring resonators play an essential role in the development of photonic integrated circuits, contributing to the design of logic gates and the realization of logical operations.

The development of photonic integrated circuits involves several fundamental processes, including filtering, routing, switching, modulation, multiplexing, and demultiplexing [1]. To create effective ring resonators that meet the standards of photonics-based integrated circuits, photonic crystals are an excellent choice. The outstanding characteristics of micro ring resonators allow the initial power to circulate within the ring cavity while it is stored and built up in the micro ring [2]. The nonlinear Kerr effect has been successfully utilized in the design of various significant optical devices, including ring resonator-based optical logic gates [3, 4], digital-to-analog converters [5], analog-to-digital converters [6-8], and 2-to-4 decoders [9]. Interference effects have been employed in research related to both the all-optical half adder [10] and the Toffoli gate [11].

Ring resonators have proven valuable across a diverse range of device applications, thanks to their strong spectrum selectivity and extensive free spectral range. In this context, “applications” encompass linear, passive devices like filters, dispersion compensators, and sensors [12-14], as well as active devices such as modulators, switches, and lasers [15], and nonlinear devices for applications in cavity quantum electrodynamics [16]. Moreover, PCRRs are a versatile and powerful type of optical resonator. PCRRs have the potential to be used in a wide range of applications, such as optical communication [17], sensing [18, 19], nonlinear optics [20], and biomedical [21]. Recent research has demonstrated a variety of distinct photonic crystal ring-shaped waveguide resonator topologies. In the hybrid PC-waveguide structure, the 90-degree bending section of the waveguide ring resonator is replaced with photonic crystal reflectors to minimize bending losses associated with typical waveguides, enabling a smaller bending radius [22]. Bending losses that depend on the size are not observed in the behavior of PCRR-based structures. Similar relationships have been identified between the effective ring radius and the group velocity associated with dispersion for the free spectral range in PCRR [23]. Based on these findings, it is suggested that PCRRs may replace the micro-ring resonators currently used for high-density photonic integration and ultra-compact WDM components [24].

In most situations, ring resonator switches were built using waveguides for input and output in addition to a ring. The resonant wavelength of these devices is determined as follows:

$$\lambda_m = \frac{n_{\text{eq}} 2\pi R}{m} \quad (1)$$

Here,  $n_{\text{eq}}$  represents the equivalent index of the waveguide,  $R$  is the ring radius, and  $m$  is an arbitrary integer.

The ideal size of the ring resonator can be determined by the desired resonant wavelength  $\lambda$  while optimizing both the quality factor  $Q$  and the total volume of the modal mode  $V$ . The direction of the coupling is primarily determined by the modal symmetry as well as the relative coupling that exists between the ring resonators [25]. Through

an analysis of the coupling direction, one can determine not only the path the wave will take through the waveguide but also the direction it will follow within the ring resonator [26].

Assuming continuous wave (CW) operation and matching fields makes it simple to derive the fundamental spectral properties of an all-pass filter (APF) ring resonator. With the assumption that there are very few reflections traveling back into the bus waveguide, the ratio of the transmitted field to the incident field is

$$T_N = \frac{E}{I} = \frac{A^2 - 2\Gamma A \cos \varphi + \Gamma^2}{1 - 2A\Gamma \cos \varphi + (\Gamma A)^2} \quad (2)$$

For continuous wave operation, transmission and reflection are the basic properties of waveguides. Considering that no back reflection is present in the ring resonator, only the transmission properties are considered for analysis [27];  $E$  is the reference signal and  $I$  is the input signal. Under critical coupling, the coupled power equals the power loss in the ring. And  $1 - \Gamma^2 = \delta^2$ ,  $\Gamma = A$ ,  $\varphi = \beta L$  represents the single-pass phase shift, where  $L$  is the round-trip length, and  $\beta$  is the propagation constant of the circulating mode.  $A$  denotes the single-pass amplitude transmission, which includes both propagation loss in the ring and losses in the couplers. It is related to the power attenuation coefficient  $\alpha$  [1/cm] as  $A^2$ .  $\Gamma$  represents the self-coupling coefficient. Similarly, we can define  $\delta$  as the cross-coupling coefficient, and  $\Gamma^2$  and  $\delta^2$  are the power splitting ratios of the coupler, and they are assumed to satisfy  $\Gamma^2 + \delta^2 = 1$ .

## 2. Ring resonator design and spectral characteristics

At least one of the waveguides in an optical ring resonator is designed to function as a closed-loop system, coupled to a source of light and a sink. Optical ring resonators operate based on phenomena like interference and total internal reflection. Light of a suitable wavelength is sent into the circular loop-like waveguide. When resonance occurs, the intensity of light builds up due to constructive interference and is found as output in a bus waveguide. Since the ring resonator permits resonance for a certain range of wavelengths and only allows them to pass through, it acts as a filter. The output bus waveguide functions as a detector waveguide. Power is transmitted from the bus waveguide to the ring waveguide through the evanescent field [28].

As shown in Fig. 1 [29], positioning the waveguide axes close to one another can change the coupling between two optical waveguides, ensuring that a wave is excited in one fiber by the evanescent field produced by the other. Evanescent wave coupling is frequently employed as a coupler in photonic and nanophotonic devices. Spectral parameters, including full width at half maximum (FWHM) and free spectral range (FSR), are directly determined from the output transmission spectrum, as illustrated in Fig. 2 [30]. Additionally, finesse  $F$  and the quality factor QF of the ring resonator are calculated using Eqs. (8) and (9).

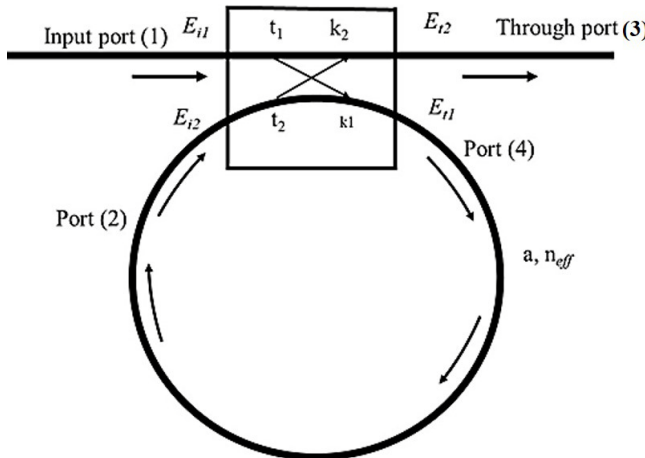


Fig. 1. All-pass ring resonator configuration.

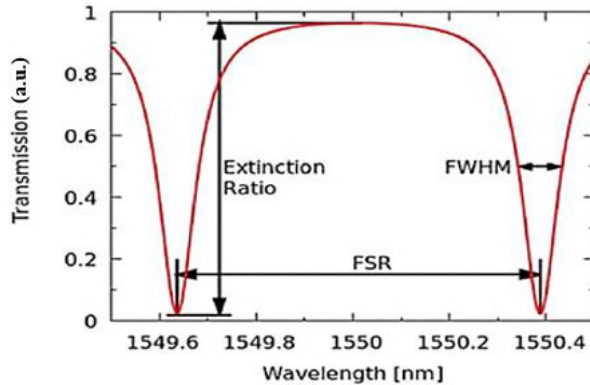


Fig. 2. Spectral response of all-pass ring resonator.

The full width half maximum (FWHM) of the resonance spectrum can be calculated as

$$\text{FWHM} = \frac{(1 - ra)\lambda_{\text{res}}^2}{\pi n_g L \sqrt{ra}} \quad (3)$$

Here  $ra$  represents the power reflectance,  $\lambda_{\text{res}}$  is the resonant wavelength,  $n_g$  is the group index, and  $L$  is the round-trip length of the ring resonator.

In the first-order approximation of dispersion, the formula for determining the free spectral range (FSR) as a function of wavelength is provided by

$$\text{FSR} = \frac{\lambda^2}{n_g L} \quad (4)$$

By considering waveguide dispersion, the group index  $n_g$  is defined by

$$n_g = n_{\text{eff}} - \lambda_0 \frac{dn_{\text{eff}}}{d\lambda} \quad (5)$$

where  $n_{\text{eff}}$  represents the effective refractive index, and  $\lambda_0$  is the center wavelength.

The group index and the corresponding group velocity can be used to relate the travel velocity of the propagating pulse envelope to the properties of the dispersive medium through the equation  $v_g = c/n_g$ , where  $v_g$  is the group velocity,  $c$  is the speed of light, and  $n_g$  is the group index.

The velocity of the propagating pulse envelope and the characteristics of the dispersive medium can be related by the group index and the corresponding group velocity through the equation  $v_g = c/n_g$ . The contrast ratio of the through port transmission is equal to  $T_t/R_{\min}$ . For an all-pass filter (APF) ring configuration, we have the transmission coefficient  $T_t$  and minimum reflection coefficient  $R_{\min}$  as

$$T_t = \frac{(r+a)^2}{(1+ra)^2} \quad (6)$$

$$R_{\min} = \frac{(r-a)^2}{(1-ra)^2} \quad (7)$$

The finesse parameter, used to characterize the spectral shape of the build-up factor, displays sharply peaked resonances. The formula for calculating the finesse, shown in Eq. (8), is the ratio of the free spectral range (FSR) between resonance peaks to the full width at half depth (FWHD) of a resonance.

$$\text{Finesse} = \frac{\text{FSR}}{\text{FWHM}} \quad (8)$$

Therefore, it measures how sharp resonances are relative to their separation. The quality factor, also known as the  $Q$ -factor and represented in Eq. (9), is used to determine how sharp a resonance is concerning its fundamental frequency.

$$Q\text{-factor} = \frac{\lambda_{\text{res}}}{\text{FWHM}} \quad (9)$$

Formally,  $Q$ -factor is defined as the ratio of the amount of energy stored and used within the resonator to the amount of energy lost during one optical cycle

$$Q\text{-factor} = \omega_0 \frac{\text{Stored energy}}{\text{Power loss}} \quad (10)$$

where  $\omega_0 = 2\pi f_0$ , angular resonant frequency.

For the numerical simulation of the all-optical ring resonator, it is important to perform a high-frequency analysis of a micro ring resonator consisting of a straight wave-

guide and micro ring cavity. Finite-difference time-domain (FDTD) can be employed for numerical simulation, as Maxwell's equations are used to describe electromagnetic waves. Assuming the horizontal direction is  $x$  and the vertical direction is  $z$ , with fields remaining constant in the  $y$ -direction, the partial derivative equations with respect to  $y$  will vanish. This leads to the splitting of Maxwell's equations (Eqs. (11)–(16)), differentiating between the TM mode and TE mode concerning  $y$  [31].

For  $\text{TM}_y$  mode (transverse magnetic mode in the  $y$ -direction),

$$\frac{\partial H_x}{\partial t} = \frac{1}{\mu} \frac{\partial E_y}{\partial z} \quad (11)$$

$$\frac{\partial H_z}{\partial t} = -\frac{1}{\mu} \frac{\partial E_y}{\partial x} \quad (12)$$

$$\frac{\partial E_y}{\partial t} = \frac{1}{\varepsilon} \frac{\partial H_x}{\partial z} - \frac{\partial H_z}{\partial x} - \mathcal{J}_y \quad (13)$$

For  $\text{TE}_y$  mode (transverse electric mode in the  $y$ -direction),

$$\frac{\partial E_x}{\partial t} = \frac{1}{\varepsilon} \left( -\frac{\partial H_y}{\partial z} - \mathcal{J}_x \right) \quad (14)$$

$$\frac{\partial E_z}{\partial t} = \frac{1}{\varepsilon} \left( \frac{\partial H_y}{\partial z} - \mathcal{J}_z \right) \quad (15)$$

$$\frac{\partial H_y}{\partial t} = \frac{1}{\mu} \left( \frac{\partial E_x}{\partial z} - \frac{\partial E_z}{\partial x} \right) \quad (16)$$

The subscripts ( $x$ ,  $y$ ,  $z$ ) indicate the spatial directions, and  $\varepsilon$  and  $\mu$  represent the permittivity and permeability of the material, respectively. The wave impedance, denoted by  $\mathcal{J}$  (usually a vector), accounts for the wave's propagation characteristics in the medium.

### 3. Design, results and discussion

The design parameters of the proposed ring resonator are listed in Table 1. The proposed design yields two bandgaps in TE mode with gap widths of 0.219233 and 0.34826  $\mu\text{m}^{-1}$ . The first bandgap falls within the range of 0.456586 to 0.675819  $\mu\text{m}^{-1}$ , while the second bandgap spans from 1.12855 to 1.16338  $\mu\text{m}^{-1}$ . The corresponding wavelengths are within the ranges of 1479 to 2190 nm and 859 to 886 nm, respectively. Within these ranges, a wavelength of 1550 nm was chosen for the ring resonator design due to its low-loss characteristics.

Corner scatter is incorporated into the ring structure, and its significance is studied by comparing the spectrum. The discrete Fourier transform (DFT), field distribution, and

Table 1. Ring resonator design parameters.

Design parameters	
Wafer dimension	$9 \times 10$
Wafer material	Air
R.I. of wafer material	1.0
Dielectric material	Silicon
R.I. of dielectric material	3.477
Lattice constant	560 nm
Lattice dimension	$17 \times 15$
Lattice type	Square lattice
Type of photonic crystal structure	Rod type
Radius of rod	$0.21a$ ( $0.118 \mu\text{m}$ )
Input parameters	
Input wave	Continuous wave
Transverse type	Rectangular
Wavelength	1550 nm
Input amplitude	1 V/m

coupling behavior were also observed. The finite-difference time-domain (FDTD) approach was used to model the suggested ring resonator design. FDTD solves Maxwell's equations in the time domain, distinguishing it from most frequency domain methods, allowing for the calculation of electromagnetic field values at discrete time points [32]. Its bandgap structure (seen in Fig. 3) was constructed using the parameters provided in Table 1 through the plane wave expansion (PWE) approach. It represents electromagnetic fields within the crystal as a sum of plane waves, helping determine the allowed

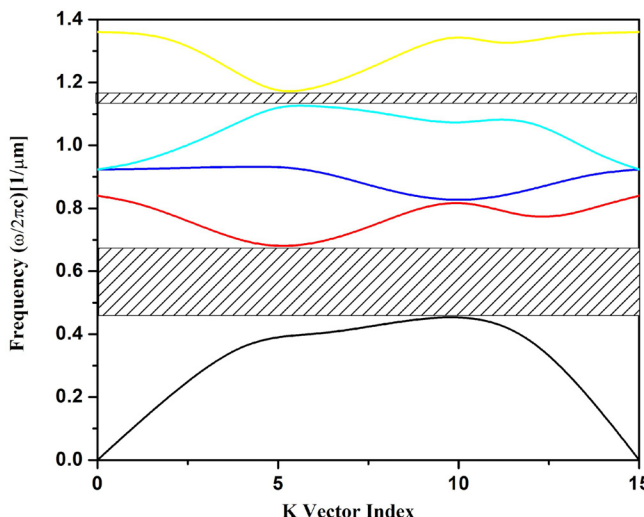


Fig. 3. The bandgap structure of the proposed ring resonator.

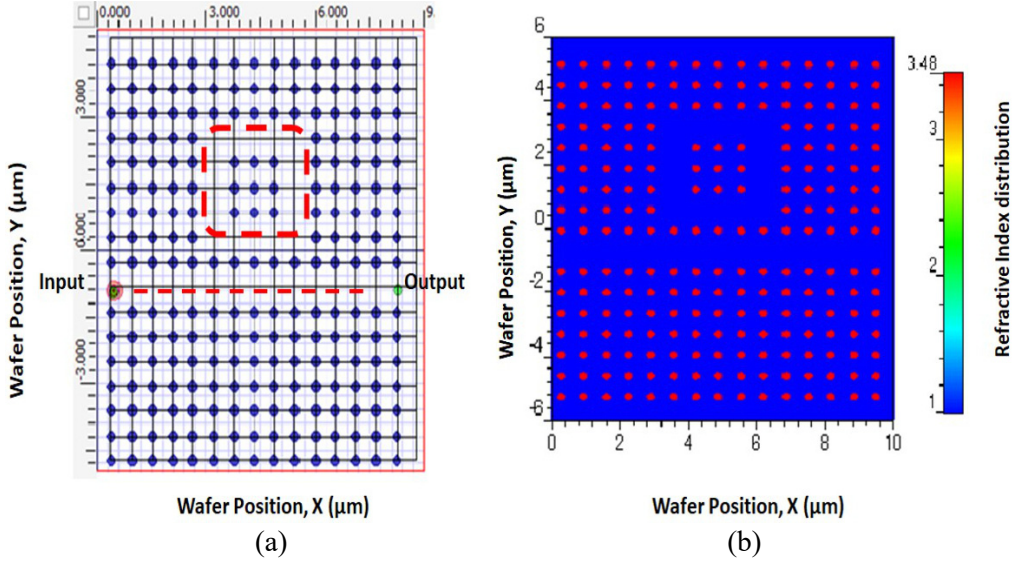


Fig. 4. (a) The design layout and (b) refractive index distribution for ring resonator.

photonic modes and their corresponding frequencies, crucial for designing photonic devices and understanding light propagation within these periodic structures [33].

A layout is created in the OptiFDTD window using the parameters listed in Table 1, which includes neatly arranged silicon rods with dimensions of  $17 \times 15$  embedded in the wafer, as depicted in Fig. 4(a). The distribution of refractive indices is shown in

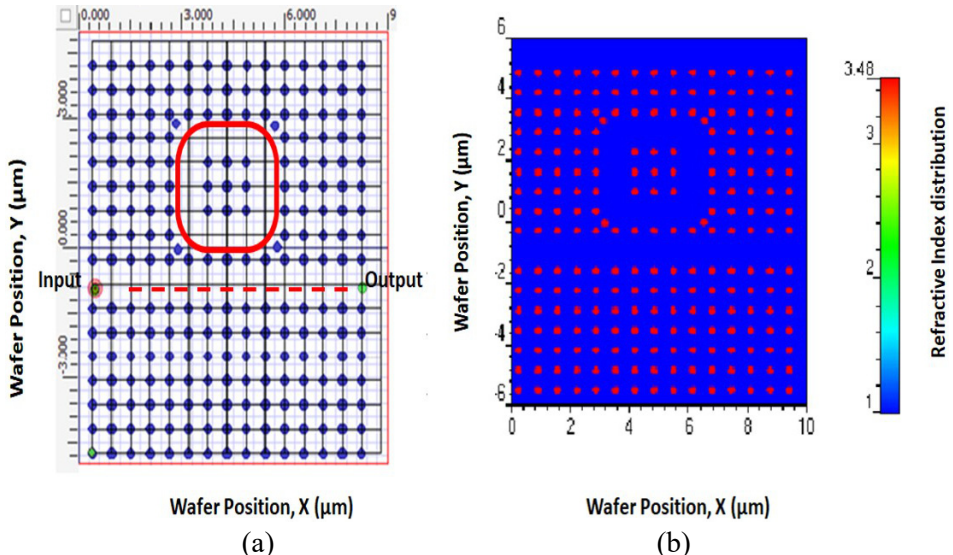


Fig. 5. (a) The modified design layout and (b) corresponding refractive index distribution for ring resonator with silicon corner scatter.

Fig. 4(b). In this design, the medium for light propagation is air. Air and silicon, which are discretely distributed throughout the region, play a critical role in the development of nonlinear properties for light propagation. This design serves as a fundamental element for the construction of various optical active and passive devices.

In terms of optimizing the gate design, the size of the rod arrangements, and the coupling of rings together play the most significant roles. The ring formation and line waveguide are indicated by a red dashed line.

Figure 5(a) and (b) show the modified version of the prior ring resonator design. In this version, all the corners of the square ring are embedded with silicon rods, making the ring more analogous to a typical circular ring. Corner scatters play an important role in guiding the field smoothly inside the ring, which significantly prevents the localization of light within the structure. By carefully engineering the scattering at the corners, it is possible to tailor the behavior of the resonator and achieve specific functionalities.

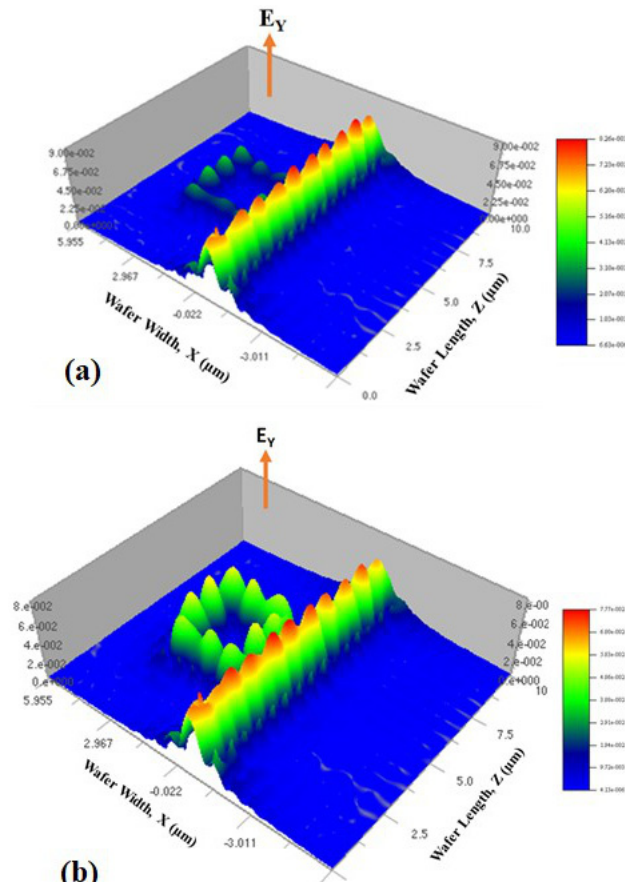


Fig. 6. The height plot of field propagation in ring resonator (a) without corner scatter and (b) with corner scatter.

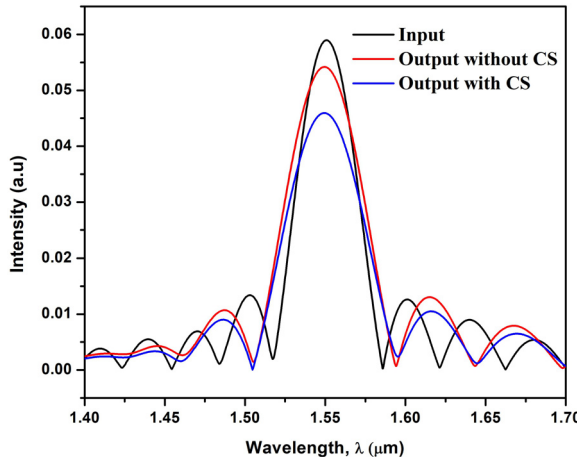


Fig. 7. The spectral relationship between input and output signals in ring resonator.

Figure 6 depicts the field propagation height plot for (a) without corner scatter and (b) with corner scatter. It is evident from Fig. 6(a) and (b) that corner dispersion plays a crucial role in achieving resonance, which improves the output of the structure.

The spectrum (DFT) of the ring resonator with and without corner scatter is shown in Fig. 7 for the configuration with corner scatter. To compute the graph with arbitrary units (a.u.), the value of  $E_y$  is used as the y-axis data. The intensity of the input signal is represented by the solid black line. The incorporation of corner scatters results in a variation in the output spectrum's intensity, as depicted by the red and blue lines in Fig. 7. At a resonant wavelength of 1550 nm, the input intensity is 0.0591 a.u., while the output intensity with and without corner scatter is 0.0458 and 0.0539 a.u., respectively. The spectral characteristics of the proposed PCRR with and without corner scatter is summarized in Table 2.

By examining the tabulated data, it is evident that the PCRR with corner scatter exhibits a narrower full width at half maximum (FWHM), a higher extinction ratio (ER), and greater finesse compared to the PCRR without corner scatter. This suggests that the PCRR with corner scatter displays an enhanced spectral response and is more proficient in capturing and retaining light.

Table 2. The measured and the calculated spectral parameters of the proposed PCRR.

Parameter	PCRR with corner scatter	PCRR without corner scatter
FWHM [nm]	0.02	0.03
ER [dB]	10	5
FSR [nm]	0.06	0.06
Finesse	3	2
Quality factor $Q$	1500	1000

## 4. Conclusions

In this proposed study, the significance of ring resonators in photonic integrated circuits is examined by comparing two distinct designs: first, a ring resonator design with silicon corner scatter, and second, a ring resonator design without corner scatter. Both designs' responses in terms of DFT spectrum and field propagation along the  $y$ -axis were observed. It is observed that the insertion of corner scatters affects the output spectrum's intensity, and their responses have been plotted. At a resonant wavelength of 1550 nm, the input intensity is 0.0591 a.u., and the output intensity with corner scatter is 0.0458 a.u., while without corner scatter, it is 0.0539 a.u. The performance of corner scatter in relation to light interactions is substantial depending on the signal conditions (logic high or low). Future designs of all-optical photonic circuits may incorporate various corner scatter materials.

## References

- [1] KUMAR V.D., SRINIVAS T., SELVARAJAN A., *Investigation of ring resonators in photonic crystal circuits*, Photonics and Nanostructures **2**(3), 2004: 199-206. <https://doi.org/10.1016/j.photonics.2004.11.001>
- [2] YANG W., JOSHI A., XIAO M., *Single-photon all-optical switching using coupled microring resonators*, Pramana – Journal of Physics **69**(2), 2007: 219-228. <https://doi.org/10.1007/s12043-007-0123-4>
- [3] YAN D., LI J., WANG Y., *Photonic crystal terahertz wave logic AND-XOR gate*, Laser Physics **30**(1), 2020: 016208. <https://doi.org/10.1088/1555-6611/ab5805>
- [4] NEFEDOV I.S., GUSYATNIKOV V.N., *Optically controlled GaAs-GaAlAs photonic band gap structure*, Journal of Optics A: Pure and Applied Optics **2**(4), 2000: 344-347. <https://doi.org/10.1088/1464-4258/2/4/318>
- [5] SRIDARSHINI T., INDIRA GANDHI S., JANNATH UI FIRTHOUSE V.N., *Compact 4-bit all optical digital to analog converter based on photonic crystal ring resonators*, Laser Physics **30**(11), 2020: 116206. <https://doi.org/10.1088/1555-6611/abbe1f>
- [6] NAGHIZADE S., SAGHAEI H., *An ultra-fast optical analog-to-digital converter using nonlinear X-shaped photonic crystal ring resonators*, Optical and Quantum Electronics **53**(3), 2021: 149. <https://doi.org/10.1007/s11082-021-02798-y>
- [7] RAMTIN FARD S., SALEHI M.R., ABIRI E., *Ultra-fast all-optical ADC using nonlinear ring resonators in photonic crystal microstructure*, Optical and Quantum Electronics **53**(2), 2021: 120. <https://doi.org/10.1007/s11082-021-02769-3>
- [8] NAGHIZADE S., SAGHAEI H., *Tunable electro-optic analog-to-digital converter using graphene nanoshells in photonic crystal ring resonators*, Journal of the Optical Society of America B **38**(7), 2021: 2127-2134. <https://doi.org/10.1364/JOSAB.423088>
- [9] MEHDIZADEH F., SOROOSH M., ALIPOUR-BANAEI H., *A novel proposal for optical decoder switch based on photonic crystal ring resonators*, Optical and Quantum Electronics **48**(1), 2016: 20. <https://doi.org/10.1007/s11082-015-0313-0>
- [10] SERAJMOHAMMADI S., ALIPOUR-BANAEI H., MEHDIZADEH F., *Proposal for realizing an all-optical half adder based on photonic crystals*, Applied Optics **57**(7), 2018: 1617-1621. <https://doi.org/10.1364/AO.57.001617>
- [11] KAZEMI M.M., TEHRANI A.M., KHAN T.Z., NAMBOODIRI M., MATERNY A., *Realization of an ultrafast all-optical Toffoli logic gate based on the phase relation between two second order nonlinear optical signals*, Laser Physics **25**(12), 2015: 125402. <https://doi.org/10.1088/1054-660X/25/12/125402>

- [12] BENMERKHI A., BOOUNIOUIA A., BOUCHEMAT M., BOUCHEMAT T., *Analysis of a photonic crystal temperature sensor based on Z-shaped ring resonator*, Optical and Quantum Electronics **53**(1), 2021: 41. <https://doi.org/10.1007/s11082-020-02730-w>
- [13] BISWAS U., RAKSHIT J.K., DAS J., BHARTI G.K., SUTHAR B., AMPHAWAN A., NAJJAR M., *Design of an ultra-compact and highly-sensitive temperature sensor using photonic crystal based single micro-ring resonator and cascaded micro-ring resonator*, Silicon **13**(3), 2021: 885-892. <https://doi.org/10.1007/s12633-020-00489-z>
- [14] PATIL P.P., KAMATH S.P., UPADHYAYA A.M., SHARAN P., *Design and analysis of photonic MEMS based micro ring resonators for pressure sensing application*, Journal of Micromechanics and Microengineering **31**(11), 2021: 115004. <https://doi.org/10.1088/1361-6439/ac2bb1>
- [15] MORADI M., MOHAMMADI M., OLYAEE S., SEIFOURI M., *Design and simulation of a fast all-optical modulator based on photonic crystal using ring resonators*, Silicon **14**(3), 2022: 765-771. <https://doi.org/10.1007/s12633-020-00891-7>
- [16] THIRUMARAN S., DHANABALAN S.S., SANNASI I.G., *Design and analysis of photonic crystal ring resonator based 6 × 6 wavelength router for photonic integrated circuits*, IET Optoelectronics **15**(1), 2021: 40-47. <https://doi.org/10.1049/ote2.12014>
- [17] MORADI M., MOHAMMADI M., OLYAEE S., SEIFOURI M., *Design and simulation of a fast all-optical modulator based on photonic crystal using ring resonators*, Silicon **14**, 2022: 1-7. <https://doi.org/10.1007/s12633-020-00891-7>
- [18] KAZANSKIY N.L., KHONINA S.N., BUTT M.A., *A review of photonic sensors based on ring resonator structures: three widely used platforms and implications of sensing applications*, Micromachines **14**(5), 2023: 1080. <https://doi.org/10.3390/mi14051080>
- [19] NOHOJI A.H.A., DANAIE M., *Highly sensitive refractive index sensor based on photonic crystal ring resonators nested in a Mach-Zehnder interferometer*, Optical and Quantum Electronics **54**(9), 2022: 574. <https://doi.org/10.1007/s11082-022-04006-x>
- [20] BLACK J.A., BRODNIK G., LIU H., YU S.P., CARLSON D.R., ZANG J., BRILES T.C., PAPP S.B., *Optical -parametric oscillation in photonic-crystal ring resonators*, Optica **9**(10), 2022: 1183-1189. <https://doi.org/10.1364/OPTICA.469210>
- [21] BISWAS U., KUMAR RAKSHIT J., *Detection and analysis of hemoglobin concentration in blood with the help of photonic crystal based micro ring resonator structure*, Optical and Quantum Electronics **52**, 2020: 449. <https://doi.org/10.1007/s11082-020-02566-4>
- [22] KOUDDAD E., NAOUM R., *Optimization of an all-optical photonic crystal NOT logic gate using switch based on nonlinear Kerr effect and ring resonator*, Sensor Letters **18**(2), 2020: 89-94. <https://doi.org/10.1166/sl.2020.4200>
- [23] QIANG Z., SOREF R.A., ZHOU W., *Photonic crystal ring resonators: Characteristics and applications*, Journal of Nanoscience and Nanotechnology **10**(3), 2010: 1495-1507. <https://doi.org/10.1166/jnn.2010.2027>
- [24] KIM S., CAI J., JIANG J., NORDIN G.P., *New ring resonator configuration using hybrid photonic crystal and conventional waveguide structures*, Optics Express **12**(11), 2004: 2356-2364. <https://doi.org/10.1364/OPEX.12.002356>
- [25] TANUSHI Y., YOKOYAMA S., *Design and simulation of ring resonator optical switches using electro-optic materials*, Japanese Journal of Applied Physics **45**(4S), 2006: 3493-3497. <https://doi.org/10.1143/JJAP.45.3493>
- [26] QIANG Z., ZHOU W., SOREF R.A., *Optical add-drop filters based on photonic crystal ring resonators*, Optics Express **15**(4), 2007: 1823-1831. <https://doi.org/10.1364/OE.15.001823>
- [27] ROBINSON S., NAKKEERAN R., *Photonic crystal ring resonator based optical filters*, [In] *Advances in Photonic Crystals*, [Ed.] V. Passaro, InTech, 2013. <https://doi.org/10.5772/54533>
- [28] RABUS D.G., SADA C., *Ring resonators: Theory and modeling*, [In] *Integrated Ring Resonators: A Compendium*, Springer Series in Optical Sciences, Vol. 127, Springer, Cham, 2020: 3-46. [https://doi.org/10.1007/978-3-030-60131-7\\_2](https://doi.org/10.1007/978-3-030-60131-7_2)

- [29] MENÉNDEZ R.J.P., *Fiber-optic ring resonator interferometer*, [In] *Interferometry-Recent Developments and Contemporary Applications*, [Eds.] M. Bhowmick, B. Ullrich, IntechOpen, 2019, p. 130. <https://doi.org/10.5772/intechopen.80569>
- [30] HENRIKSSON A., KASPER L., JÄGER M., NEUBAUER P., BIRKHOLZ M., *An approach to ring resonator biosensing assisted by dielectrophoresis: Design, simulation and fabrication*, *Micromachines* **11**(11), 2020: 954. <https://doi.org/10.3390/mi11110954>
- [31] DUARTE F.J., *Tunable Laser Optics*, CRC Press, United Kingdom, 2017.
- [32] TAFLOVE A., HAGNESS S.C., PIKET-MAY M., *Computational electromagnetics: The finite-difference time-domain method*, [In] *The Electrical Engineering Handbook*, [Ed.] Wai-kai Chen, Academic Press, 2005: 629-670. <https://doi.org/10.1016/B978-012170960-0/50046-3>
- [33] JOANNOPOULOS J.D., JOHNSON S.G., WINN J.N., MEADE R.D., *Photonic Crystals: Molding the Flow of Light*, 2nd Ed., Princeton University Press, 2008.

Received June 20, 2023  
in revised form October 23, 2023